Persistence and Predictions of the Remarkable Warm Anomaly in the Northeastern Pacific Ocean during 2014–16

ZENG-ZHEN HU AND ARUN KUMAR

Climate Prediction Center, NOAA/NWS/NCEP, College Park, Maryland

BHASKAR JHA AND JIESHUN ZHU

Climate Prediction Center, NOAA/NWS/NCEP, College Park, and Innovim, Greenbelt, Maryland

BOHUA HUANG

Center for Ocean–Land–Atmosphere Studies and Department of Atmospheric, Oceanic, and Earth Sciences, College of Science, George Mason University, Fairfax, Virginia

(Manuscript received 29 April 2016, in final form 6 September 2016)

ABSTRACT

In this work, the evolution and prediction of the persistent and remarkable warm sea surface temperature anomaly (SSTA) in the northeastern Pacific during October 2013–June 2016 are examined. Based on experiments with an atmospheric model, the possible contribution of SSTAs in different ocean basins to the atmospheric circulation anomalies is identified. Further, through verifying the real-time forecasts, current capabilities in predicting such an extreme warm event with a state-of-the-art coupled general circulation model are assessed.

During the long-lasting warm event, there were two warm maxima in the area-averaged SSTA around January 2014 and July 2015, respectively. The warm anomaly originated at the oceanic surface and propagated downward and reached about 300 m. Model experiments forced by observed SST suggest that the long persistence of the atmospheric anomalies in the northeastern Pacific as a whole may be partially explained by SST forcing, particularly in the tropical Pacific Ocean associated with a persistent warm SSTA in 2014/15 and an extremely strong El Niño in 2015/16, via its influence on atmospheric circulation over the North Pacific. Nevertheless, it was a challenge to predict the evolution of this warm event, especially for its growth. That is consistent with the fact that the SSTAs in extratropical oceans are largely a consequence of unpredictable atmospheric variability.

1. Introduction

Annual mean sea surface temperature (SST) averaged over the global ocean in 2015 surpassed 2014, and 2015 was the warmest year since 1950 (Xue et al. 2016). The historical warm anomaly of the global-averaged SST in 2015 was largely due to the extremely strong El Niño in 2015/16, but the strong warm anomalous SST in the northeastern Pacific Ocean (NEPO) was also a contributor. Large positive SST anomalies (SSTAs) emerged in NEPO during the boreal winter of 2013/14 (Bond et al. 2015a; Fig. SB3.1 of Bond et al. 2015b; Fig. 3.2d of Xue et al. 2015) and persisted to the winter of 2015/16 (Fig. 1). Bond et al. (2015a,b) refereed to this persistent warm anomalous pattern as a ''blob.'' This unprecedented warm event in the North Pacific affected the ecosystem in the Gulf of Alaska and may also be connected with seasonal weather in the Pacific Northwest, as noted in Bond et al. (2015a).

Bond et al. (2015a) suggested that the anomalous warm SST anomalies were caused by both lower than normal rates of the heat loss from the ocean to the atmosphere and relatively weak cold water advection in the upper ocean. They further attributed both the heat flux and oceanic advection anomalies to an unusually strong and persistent weather pattern with much higher than normal sea level pressure (SLP) over NEPO. Their results argued that atmospheric anomalies in NEPO played an active role in forcing the anomalous warm event in NEPO.

Corresponding author e-mail: Zeng-Zhen Hu, zeng-zhen.hu@noaa.gov

DOI: 10.1175/JCLI-D-16-0348.1

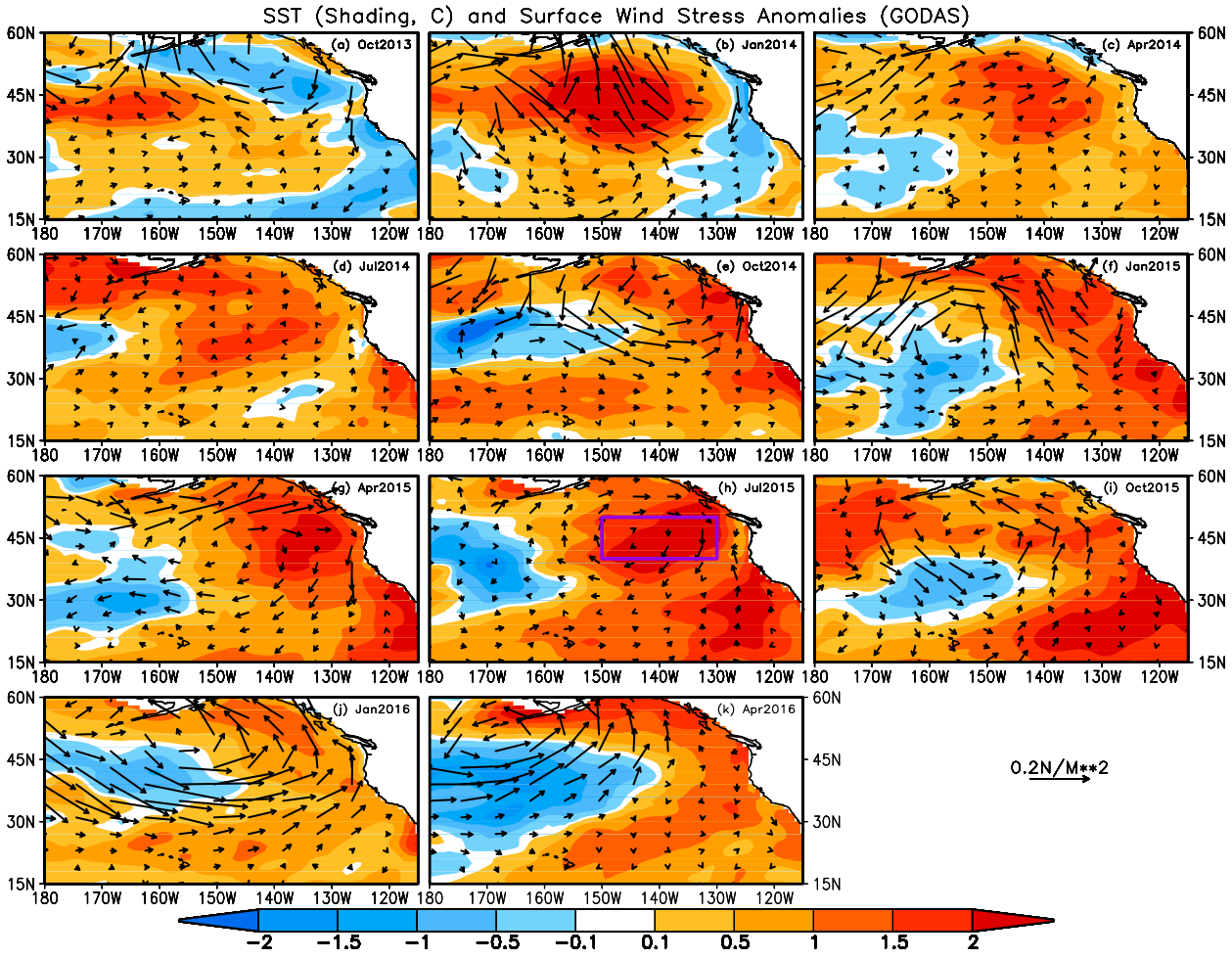

FIG. 1. (a)–(k) Monthly mean SST (shading; °C) and surface wind stress (vector; N m^{-2}) anomalies during October 2013–April 2016. The anomalies are computed based on the monthly climatology in 1982–2010. The rectangle in (h) is the region 40°–50°N, 150°–130°W referred to as the blob region in this work.

What remains unclear is the role of global SST on the persistence and reoccurrence of the atmospheric circulation anomalies in NEPO [i.e., were the persistent atmospheric anomalies a consequence of SST forcing over some remote region(s) or due to regional air–sea feedback within NEPO?] A relevant question is the following: How predictable was this long-persistent warm SSTA? In this work, through examining Atmospheric Model Intercomparison Project (AMIP)-like experiments, in which a model is forced by observed global or regional SST, we explore the possible contribution of SSTAs in different ocean basins to the atmospheric circulation anomalies. Furthermore, through analysis of real-time seasonal forecasts, we assess the possibility of predicting such extreme warm event with a state-of-the-art coupled general circulation model.

The paper is organized as follows. After describing the data and model experiments used (section 2), we discuss the evolution of atmospheric and oceanic climate anomalies and possible SST forcing from the tropics (section 3). In section 4, we evaluate real-time forecasts with a large ensemble of members and assess the possibility to predict such anomalous warm event. A summary with some discussion is given in section 5.

2. Data and model experiments

Monthly mean SLP, geopotential height at 700 hPa (H700), and wind at 1000 hPa are on a 2.5° × 2.5° resolution and from the National Centers for Environmental Prediction (NCEP)–U.S. Department of Energy (DOE) Reanalysis-2 (R2; Kanamitsu et al. 2002). Monthly oceanic surface wind stress, oceanic temperature, ocean mixed layer depth, and heat content of 0–300 m (HC300) on an 1° × 1° resolution are from the Global Ocean Data Assimilation System (GODAS; Behringer

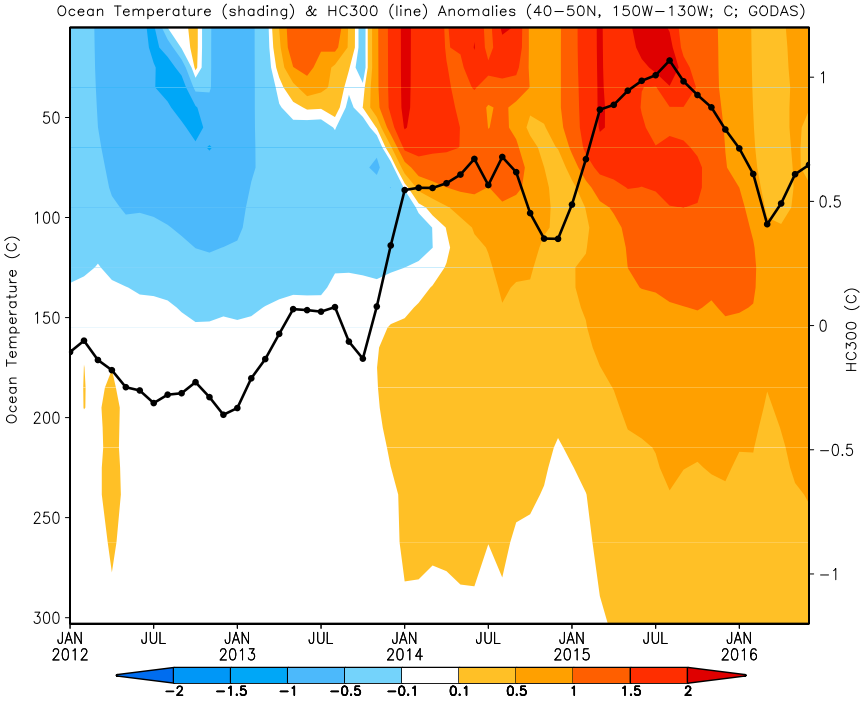

FIG. 2. Monthly mean oceanic temperature in 0–300 m (shading) and HC300 (line) anomalies (°C) averaged in the blob region (40°–50°N, 150°–130°W; see rectangle in Fig. 1h) during January 2012–June 2016. The *y* axis on the left is for oceanic depth and the *y* axis on the right is for HC300.

and Xue 2004). The oceanic mixed layer depth is defined as the depth at which the density changes within 0.125 kg m^{-3} from its surface value (Huang et al. 2010). The oceanic surface temperature in GODAS is used to represent SST. The observational and analysis data used in this work span the period from October 2013 to June 2016.

To examine the possible impact of global SST on the atmosphere, simulations with an atmospheric general circulation model (AGCM) are examined. The AGCM is the NCEP Global Forecast System (GFS), which is the atmospheric component of the NCEP Climate Forecast System, version 2 (CFSv2; Saha et al. 2014). One experiment is forced by observed global SST and sea ice, and is referred to as the AMIP run. There are 18 ensemble member integrations with slightly different atmospheric initial conditions (ICs) and the integrations are from January 1957 to May 2016. The other two experiments are forced by observed regional SST only in the global tropics (30°S–30°N; referred to as TOGA), and only in the tropical Pacific (20°S–20°N, 165°E–65°W; referred to as POGA) and a sample size of 10 ensemble members, respectively, is used. Climatological SSTs are prescribed in the remaining oceans. In our analysis, the response to extratropical SSTA is inferred in an indirect manner as the difference between the AMIP and TOGA runs. The simulated ensemble mean anomalies of SLP (SLPA) and wind at 1000 hPa are examined.

Real-time predictions are also examined and are from the NCEP CFSv2 (Kumar et al. 2012; Zhu et al. 2012; Xue et al. 2013; Jiang et al. 2013; Hu et al. 2013, 2014; Saha et al. 2014). There are four forecasts per day from the 0000, 0600, 1200, and 1800 UTC cycles of the Climate Forecast System Reanalysis (CFSR; Saha et al. 2010), out to nine months. In this analysis, predictions from 80 ICs in the last 20 days of each month are used. The atmospheric component of CFSv2 uses a spectral T126 horizontal and 64-layer vertical (T126L64) resolution, which is coupled to the Modular Ocean Model, version 4 (MOM4), as well as a three-layer sea ice model and a four-layer land model. For the ocean model, there are 40 levels in vertical, to the maximum depth of 4737 m. The horizontal resolution of MOM4 is 0.25° in the tropics, tapering to a global resolution of 0.5° poleward of 10°N and 10°S, respectively.

For comparison, corresponding to the definition in the real-time forecasts, the anomalies in the reanalyses and in the AMIP and CFS forecast runs are defined as departures from monthly climatologies in January 1982–December 2010. In addition, for the forecasts, initial condition and lead-time-dependent monthly climatologies are used.

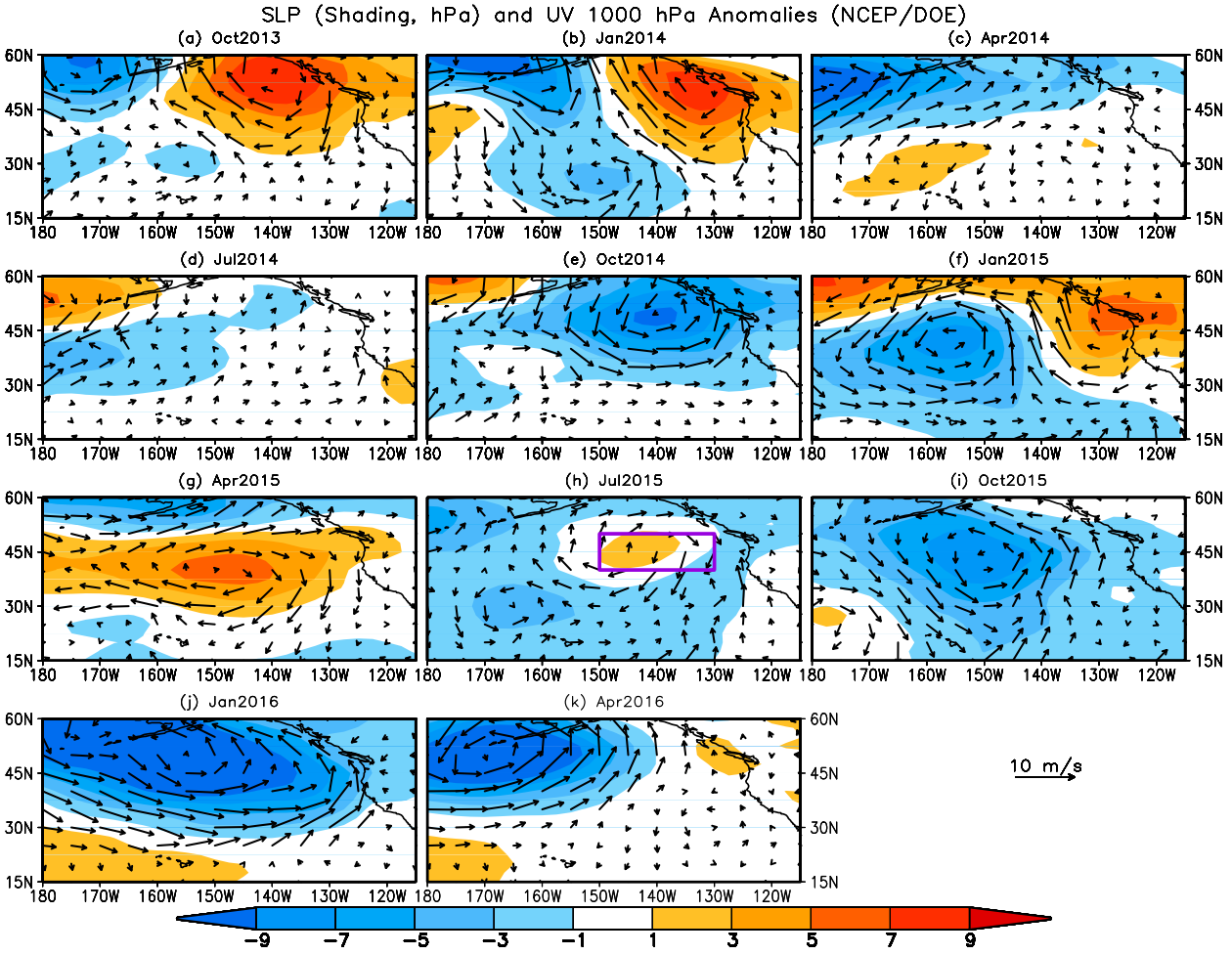

FIG. 3. As in Fig. 1, but for SLP (shading; hPa) and wind at 1000 hPa (vector; m s^{-1}) anomalies.

Through this process, the model mean drift is removed before the analysis.

3. Evolution of atmospheric and oceanic anomalies and SST forcing

a. Evolution of the atmospheric and oceanic anomalies

During October 2013–June 2016, overall positive SSTAs presented mainly along the coast and in the subtropics of NEPO with some negative SSTAs in the central ocean (Fig. 1). Such a persistent SSTA pattern may be partially associated with the dominance of the positive phase of Pacific decadal oscillation (PDO) since January 2014 (http://origin.cpc.ncep.noaa.gov/products/people/yxue/ocean_briefing_new/mnth_pdo_4yr.gif). Nevertheless, the detailed spatial pattern and the location of the maximum warming center varied with time. For example, the maximum warming was located in the Gulf of Alaska (GOA) during January–July 2014 (Figs. 1b–d). Subsequently, the maximum warm anomaly shifted along the U.S. West Coast and developed an arc shape during January–October 2015 (Figs. 1f–i). Amaya et al. (2016) and Di Lorenzo et al. (2016) referred to the former component of the warming as the GOA warming and the latter as the ARC warming. For the long-lasting NEPO warming in the so-called blob region [40°–50°N, 150°–130°W; see the rectangle in Fig. 1h; also Bond et al. (2015a)] during October 2013–June 2016, there were two maxima appearing around January 2014 and July 2015, respectively (Fig. 1).

The two anomalous peaks in the blob region are better seen from the time series of HC300 (the anomalies of averaged ocean temperature from the sea surface to 300 m) and the depth–time section of oceanic temperature averaged in the blob region (40°–50°N, 150°–130°W; see the rectangle in Fig. 1h) (Fig. 2). The warm anomaly was initiated at the ocean surface and

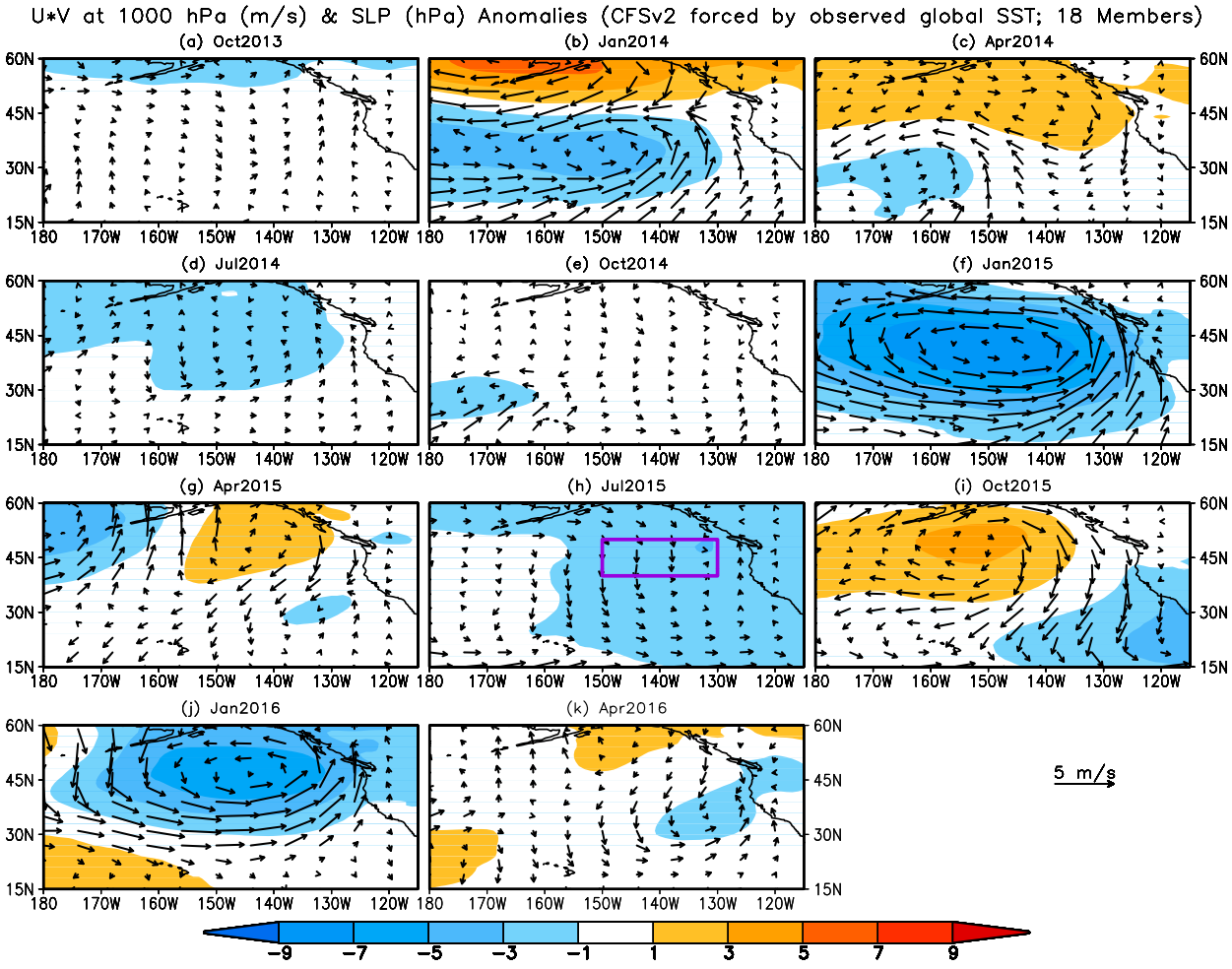

FIG. 4. (a)–(k) Monthly mean surface wind anomalies at 1000 hPa (vector) and SLP anomalies (shading) during October 2013–April 2016 of GFS simulations forced by observed global SST (AMIP run). The rectangle in (h) is the region 40°–50°N, 150°–130°W referred to as the blob region in this work.

propagated downward to reach about 300 m (shading in Fig. 2). The surface initiation and the downward propagation of warm temperature anomalies was consistent with the fact that the ocean anomaly is driven by thermodynamical processes (Bond et al. 2015a) dominated by heat exchange in the air–sea interface (e.g., Hu et al. 2011).

The atmospheric and oceanic anomalies in NEPO evolved coherently during October 2013–June 2016 (Fig. 1). Persistent positive SSTAs were collocated with an overall southerly low-level wind anomaly (Fig. 1). As demonstrated in Bond et al. (2015a), such an atmospheric circulation favored an anomalously warm advection by the anomalous Ekman flow, which was an important contributor to the warm anomaly in NEPO, in addition to the contribution of heat flux. The low-level wind anomalies in NEPO were consistent with the SLPAs (shading in Fig. 3) [i.e., a cyclonic (anticyclonic) anomalous circulation linked to negative (positive) SLPA].

b. *SST forcing on the atmosphere*

To assess the possible influence of SST in constraining atmospheric circulation, we examine the responses of SLPA and wind anomaly at 1000 hPa in the AMIP, TOGA, and POGA simulations. From the AMIP run (Fig. 4), we note the similarity of the SLPA pattern in NEPO for some periods with the corresponding observations (Fig. 3). For example, in January 2015 (Figs. 3f, 4f), April 2015 (Figs. 3g, 4g), and January 2016 (Figs. 3j, 4j), both the SLPA and low-level wind anomaly in NEPO show some similarity between the observations and simulations, implying a possible impact of global SST anomaly on the atmospheric circulation anomaly in NEPO. However, it should be pointed out that the amplitude of the wind anomaly is smaller in the model

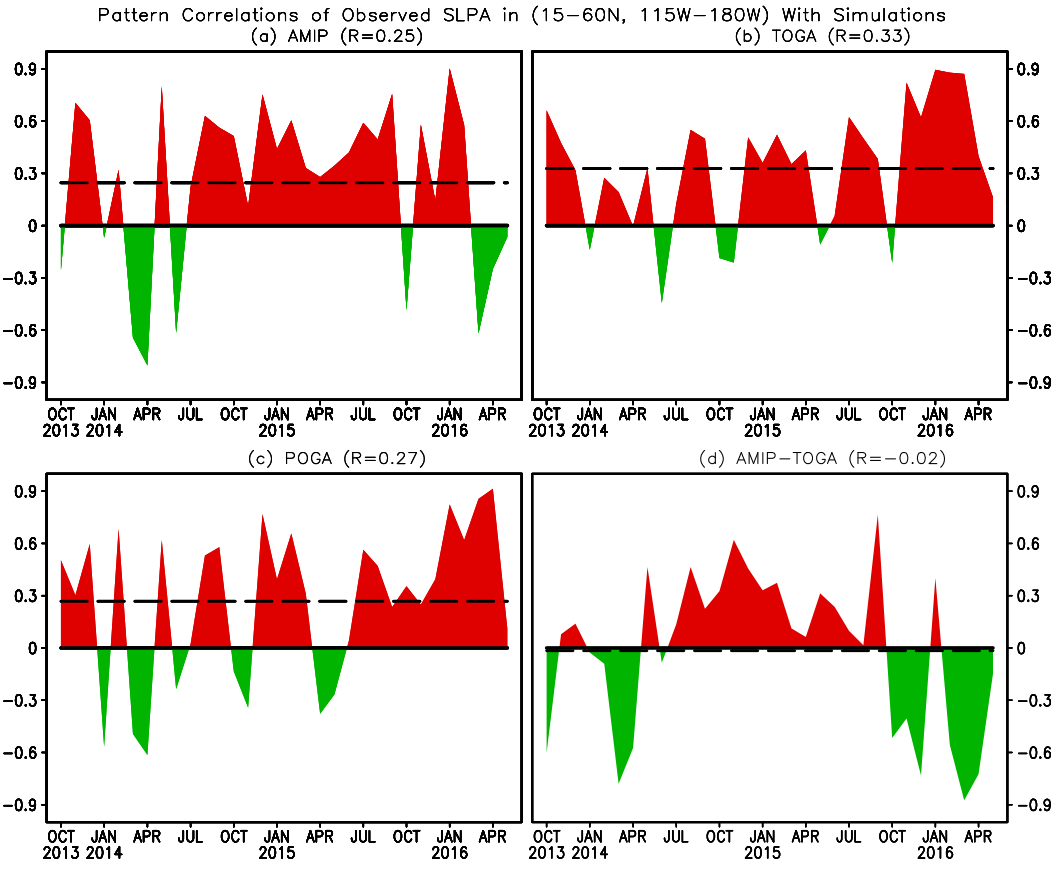

FIG. 5. Pattern correlations of observed SLPA (see Fig. 3) in 15°–60°N, 115°–180°W with simulated SLPA forced by observed SST in the (a) global (AMIP), (b) global tropical (TOGA), (c) tropical Pacific (POGA), and (d) extratropical (AMIP–TOGA) oceans. The dashed lines (and the numbers in parentheses in each panel subtitle) are the mean pattern correlations averaged in October 2013–May 2016.

simulations (Fig. 4) than in the observations (Fig. 3) (the scale of wind vector in the model simulations is half of that in the observations). Also, as the AMIP ensemble mean is an estimate of the SST-forced component, the marked differences in both the spatial distribution and amplitude between Figs. 4 and 3 suggest that maybe only a fraction of the observed variability in NEPO was forced by the SSTA while a large amount of the observed variability may have been a consequence of the atmospheric internal variability (noise). That is consistent with the conclusion from some recent work in examining the climate variability in the mid- and high latitudes of the Northern Hemisphere, such as Baxter and Nigam (2015), Hartmann (2015), Lee et al. (2015), Seager et al. (2015), Watson et al. (2016), and Jha et al. (2016).

The time evolution of the pattern similarity between the observations and the AMIP runs are seen more clearly through pattern correlation in the NEPO region (15°–60°N, 115°W–180°) (Fig. 5a). In the pattern correlation calculation, the area mean in the domain is not removed. The pattern correlations are mostly positive, except in January 2014, March–April 2014, June 2014, October 2015, and March–June 2016. The results are similar but with decreased amplitude if the SLPA evolution (tendency) is used (Fig. 6a). The decreased amplitudes of the pattern correlations suggest that compared with the anomaly itself, the anomaly evolution (tendency) seems even less similar between the observations and the simulations.

The dominance of the positive pattern correlations (Figs. 5a, 6a) confirms that SST forcing may have played a role in maintaining the atmospheric circulation anomaly over NEPO. Nevertheless, we should point out that the pattern correlation coefficients do not measure the amplitude difference between the observation and the simulation. For example, in October 2014, the observations showed a strong anomalous Aleutian low (Fig. 3e), while the simulated anomalies are very weak (Fig. 4e), although their pattern correlation was high (Figs. 5a, 6a). The remarkable amplitude differences between the observations (Fig. 3) and the simulations (Fig. 4), plus the large fluctuation of the pattern

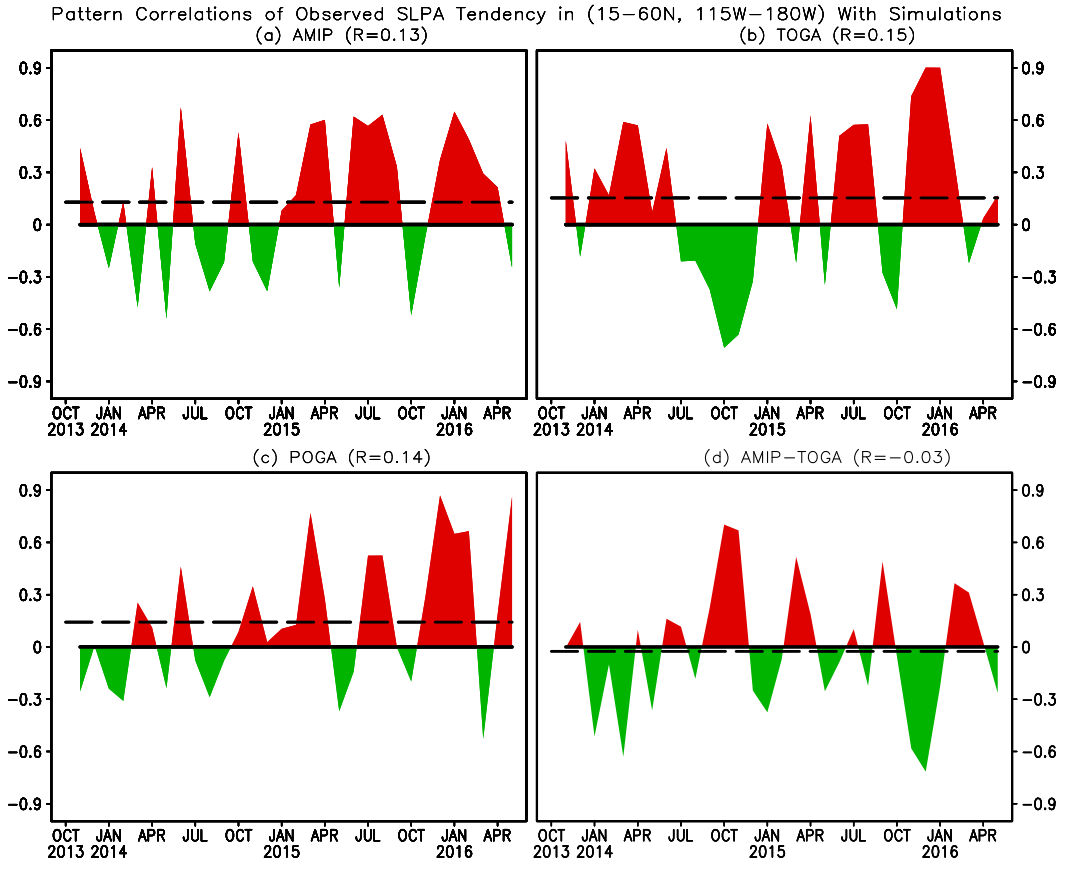

FIG. 6. As in Fig. 5, but for tendency of SLPA.

correlation (Figs. 5a, 6a), are indicative of the importance of the atmospheric internal variability (noise) in driving the observed anomalies in NEPO.

Further analysis based on simulations forced by global and regional SST indicates that the responsible SST forcing was mainly from the tropical oceans (TOGA simulation), especially the tropical Pacific Ocean (POGA simulation). This is evidenced by the high similarity among the AMIP (Fig. 4), TOGA (Fig. 7), and POGA (not shown) results. For example, between Figs. 4 and 7, the anomaly patterns of both SLP and wind at 1000 hPa are similar or almost identical in April 2014 (Figs. 4c, 7c), July 2014 (Figs. 4d, 7d), January 2015 (Figs. 4f, 7s), and July 2015 –April 2016 (Figs. 4h–k, 7h–k). The dominant role of the tropical Ocean (particularly, the tropical Pacific Ocean) in driving the total SST-forced atmospheric variability is also supported by the pattern correlations shown in Figs. 5 and 6.

The model simulations can also be used to infer the role of local or extratropical SST in forcing atmospheric circulation over NEPO in an indirect manner, which is estimated by the difference between the AMIP and POGA runs, and is found to be less important. In contrast, SST forcing in the tropical oceans (particularly the tropical Pacific Ocean) plays a more important role in constraining the atmospheric circulation anomalies. That is consistent with previous work (such as Schneider et al. 2003) and also supported by the mean pattern correlations. Specifically, for the SLPA (Fig. 5), the mean pattern correlation between the observations and simulations in the NEPO region (15°–60°N, 115°W–180°) averaged over October 2013–April 2016 is 0.25 for AMIP, 0.33 for TOGA, 0.27 for POGA, and −0.02 for AMIP–TOGA. The dominant role of the tropical Pacific is further supported when the tendency of SLPA is measured. Except for the correlation of −0.03 for AMIP–TOGA, the other three pattern correlations are between 0.13 and 0.15 (Fig. 6). We should point out that the smaller correlations in AMIP–TOGA might be different from what will be derived when the true extratropical SST forces the AGCM. There might be some nonlinearity between the responses from the tropical and extratropical SSTs, as well as in their interactions within the atmosphere.

It should be pointed out that the relatively small ensemble size might quantitatively affect the results here

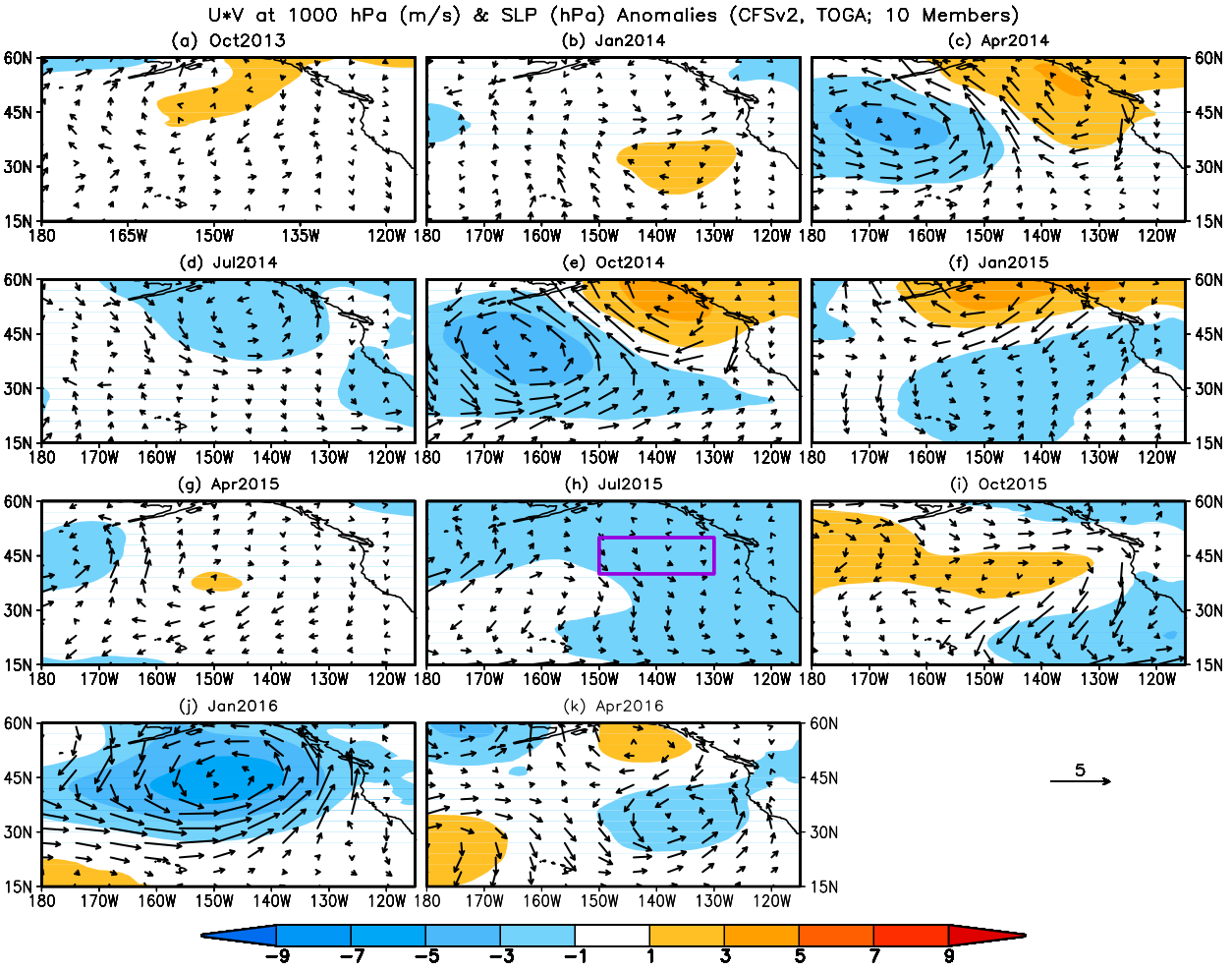

FIG. 7. As in Fig. 4, but forced by observed SST only in TOGA.

to some extent. The adequacy of inferring robust atmospheric response to SSTs has been discussed by Kumar and Hoerling (1995) and Kumar and Chen (2015). For example, Kumar and Hoerling (1995) stated that "...This [the analysis] suggests that an ensemble size of 6-10 may be sufficient to detect the boundary forced signal..." (p. 343). So although, an increase in ensemble size will improve the statistical significance of smaller-amplitude signals, large-amplitude signals to SSTs should be detectable easily based on an ensemble size of 10.

It had been demonstrated that SSTAs in the midlatitude northern oceans are affected by those in the tropical Pacific through the so-called atmospheric bridge, with the tropically induced atmospheric fluctuations altering oceanic surface heat flux over the midlatitude ocean (Alexander 1990; Lau and Nath 1996; Alexander et al. 2002; Schneider et al. 2003). The analysis here also suggests that the anomalies in NEPO were only partially constrained by the anomalously warm tropical Pacific associated with a borderline El Niño in 2014/15 and an extremely strong El Niño in 2015/16 (Xue et al. 2015, 2016). The long-persistent above-normal SST from the tropical Pacific may modulate the persistence and intensity of the atmospheric and oceanic anomalies in NEPO (Hoerling and Kumar 2002). That may provide some predictability for the anomalies in NEPO and is discussed in the next section.

4. Real-time prediction

Compared with the prediction skill in the tropical Pacific SSTs associated with El Niño–Southern Oscillation (ENSO) (Xue et al. 2013), prediction skills in the extratropical northern ocean and atmosphere are much lower (Hu and Huang 2006; Wen et al. 2012; Hu et al. 2013, 2014), and it is a challenge to skillfully predict SST anomalies in the midlatitude oceans. An assessment of

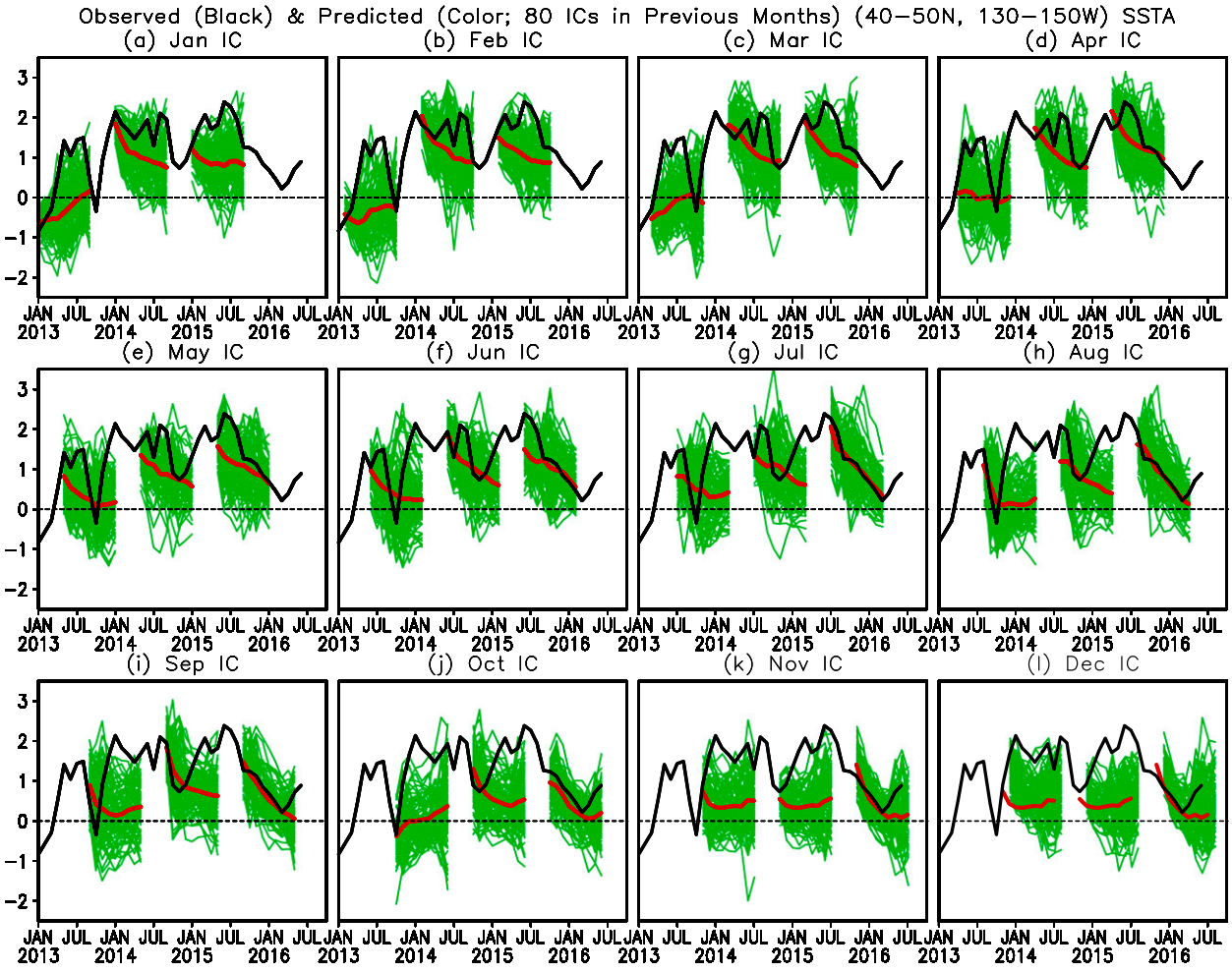

FIG. 8. CFSv2 real-time forecast SST anomalies (°C) averaged in the blob region 40°–50°N, 150°–130°W with 80 ensemble members of each month (green curves). Red curves are the ensemble means and the black curves represent the corresponding observations.

real-time prediction of CFSv2 for NEPO here also demonstrates limited skill in predicting the evolution of NEPO SSTAs despite their large amplitude.

From Fig. 8, we note that the spread among the ensemble members for SST prediction grows rapidly with forecast lead time, implying a low signal-to-noise ratio and low predictability. Even for the prediction at zero-month lead (referred to as the prediction of next month following the initial condition month), the spread among forecasts is already appreciable. This may be due to the fact that the SST anomaly in NEPO is mostly controlled by atmospheric variability that is dominated by stochastic processes, and is only weakly constrained by the evolution of SSTs in the tropical oceans (Bjerknes 1969; Hasselmann 1976; Kumar et al. 2013; Hu et al. 2014). That is consistent with the substantial spread of the atmospheric variables among individual ensemble members, such as geopotential height at 700 hPa shown in Fig. 9. As a result, SST prediction with a short lead time (such as in a month) also results in pronounced differences. In fact, tremendous differences between the observed and predicted SSTs are seen even for the first month (zero-month lead) predictions of ensemble means of 80 members (Fig. 10).

The ensemble means clearly show an overall damping tendency for all predictions with a somewhat surprisingly consistent decay among different runs (Fig. 10). With the increase of the lead time, the amplitudes of predicted anomalies (either positive or negative) decrease toward zero, implying that for ensemble mean prediction negative feedbacks or damping of the initial SST anomalies toward climatology surpasses any positive feedbacks or growth mechanisms. For example, the forecasts failed to predict the SSTA growth (such as those initiated in early 2013 and winter 2013/14), while they were relatively successful for the decay of SSTA

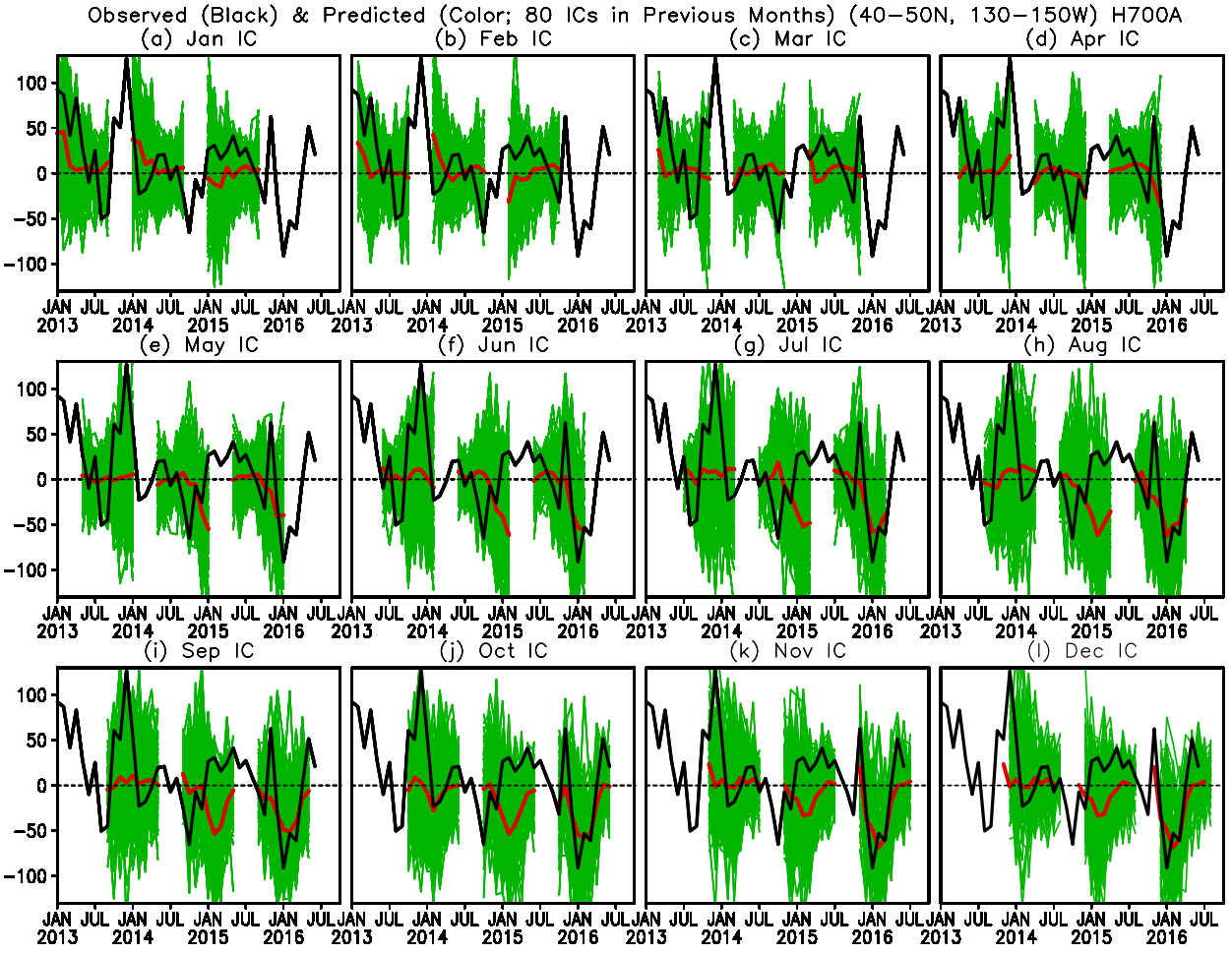

FIG. 9. As in Fig. 8, but for the geopotential height at 700 hPa (gpm).

(such as those initiated from July to December 2015). Furthermore, from Figs. 9 and 11, we note that the ensemble mean of predicted H700 anomaly is small except for the two periods around winter 2014/15 and winter 2015/16, which are associated with a borderline El Niño in winter 2014/15 and an extremely strong El Niño in winter 2015/16, respectively. The large ensemble mean anomalies in the two periods correspond to relatively higher pattern correlations shown in Figs. 5a–c. The overall small anomaly of the ensemble mean H700 in the non-ENSO periods is due to the cancelations among the individual ensemble members, which are largely generated by internal dynamical processes. With lack of consistent atmospheric forcing on average, this leads to an overall damping tendency of the SSTA prediction shown in Figs. 8 and 10.

The results here are consistent with Peng et al. (2011) that, for long lead predictions, the probability density function (PDF) of the ensemble mean of predictions would converge to the climatological PDF. As also argued by Kumar and Wang (2015), due to the fundamental property of coupled evolution of the oceanic–atmospheric system in the extratropical ocean, SSTs are driven by stochastic atmospheric variability, and without consistent atmosphere forcing within individual member predictions, the prediction of ensemble mean SST anomaly would damp toward the climatology. Therefore, the challenge of skillful prediction of SST anomaly growth in the extratropical ocean is a fundamental outcome of the nature of air–sea coupling over the extratropical oceans.

5. Discussion and conclusions

A persistent and remarkable warm anomaly occurred in the northeastern Pacific during October 2013–June 2016. This event affected the ecosystem in the Gulf of Alaska and may also be connected with the seasonal weather pattern in the Pacific Northwest and was referred to as the "blob" (Bond et al. 2015a,b). In this

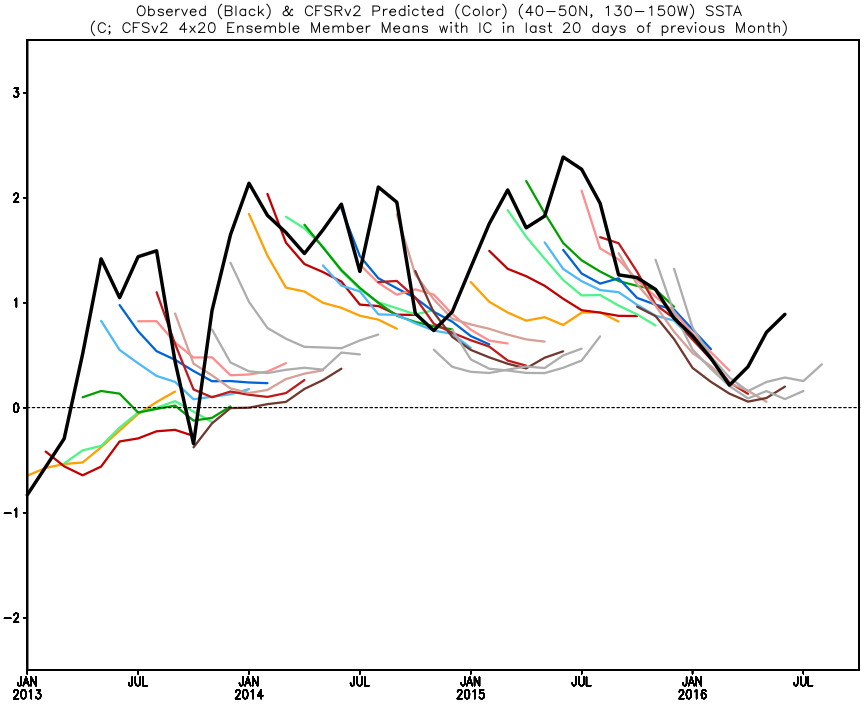

FIG. 10. As in Fig. 8, but for the ensemble mean of 80 ensemble members.

work, we further examined the evolution of the warm event, and the possible impact of tropical SST anomaly on the persistence and reoccurrence of the atmospheric circulation anomalies in the northeastern Pacific that may act as the forcing for the evolution of the warm SST anomalies. Through examining experiments with an atmospheric general circulation model, we identified possible contributions of the SSTAs in different ocean basins to the atmospheric circulation anomalies. Last, we verified the real-time forecasts against the observations and evaluated the possibility of predicting such an extreme warm event with a state-of-the-art coupled general circulation model.

During this warm event, two maxima in SST occurred in the blob region around January 2014 and July 2015, respectively. The warm anomaly initiated at the oceanic surface and propagated downward reaching about 300 m. The warm SSTA was collocated with an overall southerly low-level wind anomaly that favored anomalously warm advection. Model experiments forced by observed SST suggested that the long persistence of the anomalies in the northeastern Pacific as a whole may be partially caused by SST forcing. This result was consistent with the connection between the tropical Pacific and North Pacific suggested previously (e.g., Newman et al. 2016; Hu and Huang 2009). Among the ocean basins, the tropical oceans, particularly the tropical Pacific Ocean, played a dominant role, while the other oceans, including the local ocean anomalies over NEPO were less important in forcing atmospheric anomalies.

In the observations, the warm SST anomaly in the tropical Pacific persisted during October 2013–June 2016. In fact, a borderline El Niño was observed in 2014/15 and an extremely strong El Niño occurred in 2015/16 (Xue et al. 2015, 2016). Such SSTAs in the tropical Pacific favor the persistence of atmospheric and oceanic anomalies in the northeastern Pacific, as well as in the North America (Hartmann 2015). Recently, Amaya et al. (2016) and Di Lorenzo et al. (2016) argued that the 2014–16 NEPO warming can be separated into two components: one centered in the Gulf of Alaska (GOA) and the other along the U.S. West Coast that showed an arc shape (ARC; see Fig. 1 of Amaya et al. 2016). As mentioned in section 3, the GOA warming occurred mainly during January–July 2014 and the ARC warming merged mainly during January–October 2015 (Fig. 1). The ARC warming was suggested to be partially induced by the 2015/16 El Niño, but the GOA warming may not be significantly related to the forcing from the El Niño event (see Fig. 3 of Di Lorenzo et al. 2016). Thus, the atmospheric circulation pattern associated with the early part of the warming (i.e., the GOA warming during January–July 2014) is not related to the El Niño event and may be more stochastic in nature, while the circulation pattern associated with the latter part of the warming (i.e., the ARC warming during

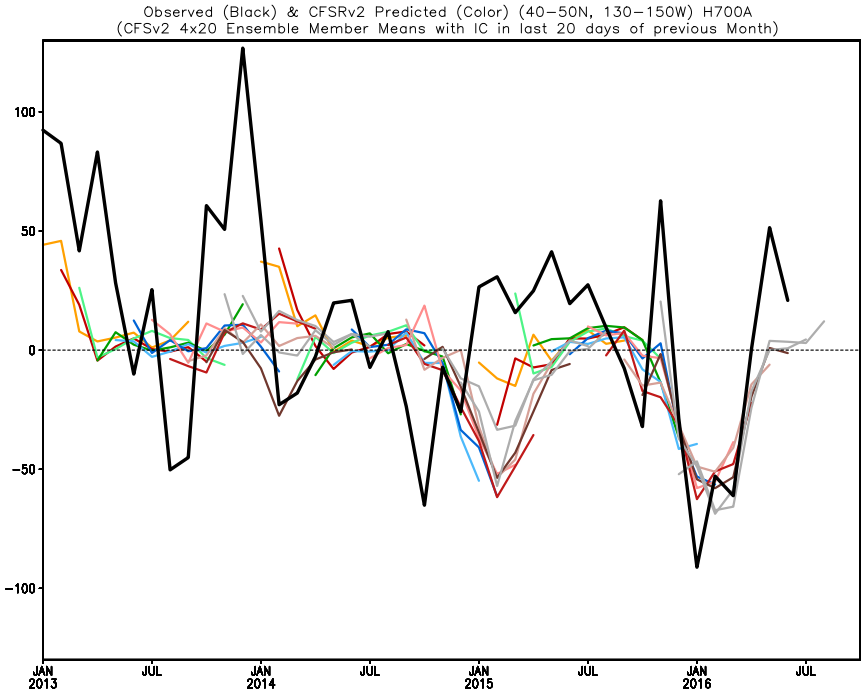

FIG. 11. As in Fig. 10, but for the geopotential height at 700 hPa (gpm).

January–October 2015) was more a consequence of the forcing from the 2015/16 El Niño and thus more predictable. This is consistent with the result shown in Figs. 5 and 6 that the pattern correlation was lower during the former period (January–July 2014) but was persistently higher during the latter period and even after October 2015, probably due to the simultaneous and lagged impact of the 2015/16 strong El Niño.

However, although the SST evolution associated with ENSO in the tropical Pacific was well predicted by CFSv2 and other dynamical seasonal prediction models (http://iri.columbia.edu/wp-content/uploads/2016/06/ensofcst_dynam_Jun16_l-1.gif), it was a challenge to predict the persistent SST anomalies in the northeastern Pacific because the SST anomaly in NEPO is largely controlled by unpredictable stochastic atmosphere variability. The ensemble mean of predictions from CFSv2 clearly showed an overall damping tendency for all predictions, implying that negative feedbacks or damping surpassed any positive feedbacks or growth mechanisms. This tendency for predictions was consistent to the fundamental property of coupled evolution of the ocean–atmosphere system in the extratropical ocean (Hasselmann 1976; Kumar and Wang 2015).

The poor prediction ability for the SST anomalous growth in the northeastern Pacific implies that the forcing from the tropical oceans is small, although it presents at some extent as we noted from the AMIP-like experiments. Furthermore, the model experiments (see Figs. 5d, 6d) suggest that the impact of local (mid-to-high latitude) SST forcing on the atmosphere is almost ignorable. Thus, the impact of the so-called blob-related SST anomalies on the air temperatures downstream over Washington State (Bond et al. 2015a) is probably due to the persistent (stochastic) atmospheric circulation pattern over the region. For example, the high pressure over the northeastern Pacific could both force warm SST anomalies to form in the northeastern Pacific–Gulf of Alaska and advect warm air over the northwestern United States. The extratropical SSTs may not be the main source of the correlation between extratropical SSTs and air temperature in Washington State, but both were responding to the atmospheric circulation.

In addition to the dominant role of thermodynamical processes during the anomalous warm event in the northeastern Pacific, some dynamical processes, such as the reemergence mechanism (Namias and Born 1970; Alexander and Deser 1995), may also have affected the persistence and evolution of the warm event. For example, from Fig. 2 as well as the mixed layer depth anomaly evolution (not shown), we note that positive temperature anomalies around January 2014 extended over the deeper ocean and were stored beneath the surface in spring and summer, which then reappeared at the sea surface in the following autumn (September and October 2015). The process seems to resemble the so-called reemergence mechanism.

Acknowledgments. We appreciate the constructive comments and suggestions from reviewers and the assistance of Dr. Wanqiu Wang in processing the CFSv2 real-time forecast data. Bohua Huang is supported by grants from NSF (Grant AGS-1338427), NOAA (Grant NA14OAR4310160), and NASA (Grant NNX14AM19G). The scientific results and conclusions, as well as any view or opinions expressed herein, are those of the authors and do not necessarily reflect the views of NWS, NOAA, or the U.S. Department of Commerce.

REFERENCES

Alexander, M. A., 1990: Simulation of the response of the North Pacific Ocean to the anomalous atmospheric circulation associated with El Niño. *Climate Dyn.*, **5**, 53–65, doi:10.1007/BF00195853.

——, and C. Deser, 1995: A mechanism for the recurrence of wintertime midlatitude SST anomalies. *J. Phys. Oceanogr.*, **25**, 122–137, doi:10.1175/1520-0485(1995)025<0122:AMFTRO>2.0.CO;2.

——, I. Bladé, M. Newman, J. R. Lanzante, N.-C. Lau, and J. D. Scott, 2002: The atmospheric bridge: The influence of ENSO teleconnections on air–sea interaction over the global oceans. *J. Climate*, **15**, 2205–2231, doi:10.1175/1520-0442(2002)015<2205:TABTIO>2.0.CO;2.

Amaya, D. J., N. E. Bond, A. J. Miller, and M. J. DeFlorio, 2016: The evolution and known atmospheric forcing mechanisms behind the 2013–2015 North Pacific warm anomalies. U.S. CLIVAR Variations, No. 14, International CLIVAR Project Office, Southampton, United Kingdom, 1–6.

Baxter, S., and S. Nigam, 2015: Key role of North Pacific Oscillation–West Pacific pattern in generating the extreme 2013/14 North American winter. *J. Climate*, **28**, 8109–8117, doi:10.1175/JCLI-D-14-00726.1.

Behringer, D. W., and Y. Xue, 2004: Evaluation of the global ocean data assimilation system at NCEP: The Pacific Ocean. *Eighth Symp. on Integrated Observing and Assimilation Systems for Atmosphere, Oceans, and Land Surface*, Seattle, WA, Amer. Meteor. Soc., 2.3. [Available online at https://ams.confex.com/ams/84Annual/techprogram/paper_70720.htm.]

Bjerknes, J., 1969: Atmospheric teleconnections from the equatorial Pacific. *Mon. Wea. Rev.*, **97**, 163–172, doi:10.1175/1520-0493(1969)097<0163:ATFTEP>2.3.CO;2.

Bond, N. A., M. F. Cronin, H. Freeland, and N. Mantua, 2015a: Causes and impacts of the 2014 warm anomaly in the NE Pacific. *Geophys. Res. Lett.*, **42**, 3414–3420, doi:10.1002/2015GL063306.

——, ——, and ——, 2015b: The blob: An extreme warm anomaly in the northeast Pacific [in "State of the Climate in 2014"]. *Bull. Amer. Meteor. Soc.*, **96** (7), S62–S63.

Di Lorenzo, E., G. Liguori, and N. Mantua, 2016: Climate interpretation of the North Pacific marine heatwave of 2013–2015. U.S. CLIVAR Variations, No. 14, International CLIVAR Project Office, Southampton, United Kingdom, 13–18.

Hartmann, D., 2015: Pacific sea surface temperature and the winter of 2014. *Geophys. Res. Lett.*, **42**, 1894–1902, doi:10.1002/2015GL063083.

Hasselmann, K., 1976: Stochastic climate models, Part 1: Theory. *Tellus*, **28A**, 473–485, doi:10.1111/j.2153-3490.1976.tb00696.x.

Hoerling, M. P., and A. Kumar, 2002: Atmospheric response patterns associated with tropical forcing. *J. Climate*, **15**, 2184–2203, doi:10.1175/1520-0442(2002)015<2184:ARPAWT>2.0.CO;2.

Hu, Z.-Z., and B. Huang, 2006: On the significance of the relationship between the North Atlantic Oscillation in early winter and Atlantic sea surface temperature anomalies. *J. Geophys. Res.*, **111**, D12103, doi:10.1029/2005JD006339.

——, and ——, 2009: Interferential impact of ENSO and PDO on dry and wet conditions in the U.S. Great Plains. *J. Climate*, **22**, 6047–6065, doi:10.1175/2009JCLI2798.1.

——, A. Kumar, B. Huang, Y. Xue, W. Wang, and B. Jha, 2011: Persistent atmospheric and oceanic anomalies in the North Atlantic from summer 2009 to summer 2010. *J. Climate*, **24**, 5812–5830, doi:10.1175/2011JCLI4213.1.

——, ——, ——, W. Wang, J. Zhu, and C. Wen, 2013: Prediction skill of monthly SST in the North Atlantic Ocean in NCEP Climate Forecast System version 2. *Climate Dyn.*, **40**, 2745–2756, doi:10.1007/s00382-012-1431-z.

——, ——, ——, J. Zhu, and Y. Guan, 2014: Prediction skill of North Pacific variability in NCEP Climate Forecast System version 2: Impact of ENSO and beyond. *J. Climate*, **27**, 4263–4272, doi:10.1175/JCLI-D-13-00633.1.

Huang, B., Y. Xue, D. Zhang, A. Kumar, and M. J. McPhaden, 2010: The NCEP GODAS ocean analysis of the tropical Pacific mixed layer heat budget on seasonal to interannual time scales. *J. Climate*, **23**, 4901–4925, doi:10.1175/2010JCLI3373.1.

Jha, B., A. Kumar, and Z.-Z. Hu, 2016: An update on the estimate of predictability of seasonal mean atmospheric variability using North American Multi-Model Ensemble. *Climate Dyn.*, doi:10.1007/s00382-016-3217-1, in press.

Jiang, X., S. Yang, Y. Li, A. Kumar, X. Liu, Z. Zuo, and B. Jha, 2013: Seasonal-to-interannual prediction of the Asian summer monsoon in the NCEP Climate Forecast System version 2. *J. Climate*, **26**, 3708–3727, doi:10.1175/JCLI-D-12-00437.1.

Kanamitsu, M., W. Ebisuzaki, J. Woollen, S.-K. Yang, J. J. Hnilo, M. Fiorino, and G. L. Potter, 2002: NCEP–DOE AMIP-II reanalysis (R-2). *Bull. Amer. Meteor. Soc.*, **83**, 1631–1643, doi:10.1175/BAMS-83-11-1631.

Kumar, A., and M. P. Hoerling, 1995: Prospects and limitations of seasonal atmospheric GCM predictions. *Bull. Amer. Meteor. Soc.*, **76**, 335–345, doi:10.1175/1520-0477(1995)076<0335:PALOSA>2.0.CO;2.

——, and M. Chen, 2015: Inherent predictability, requirements on the ensemble size, and complementarity. *Mon. Wea. Rev.*, **143**, 3192–3203, doi:10.1175/MWR-D-15-0022.1.

——, and H. Wang, 2015: On the potential of extratropical SST anomalies for improving climate predictions. *Climate Dyn.*, **44**, 2557–2569, doi:10.1007/s00382-014-2398-8.

——, M. Chen, L. Zhang, W. Wang, Y. Xue, C. Wen, L. Marx, and B. Huang, 2012: An analysis of the nonstationarity in the bias of sea surface temperature forecasts for the NCEP Climate Forecast System (CFS) version 2. *Mon. Wea. Rev.*, **140**, 3003–3016, doi:10.1175/MWR-D-11-00335.1.

——, H. Wang, W. Wang, Y. Xue, and Z.-Z. Hu, 2013: Does knowing the oceanic PDO phase help predict the atmospheric anomalies in subsequent months? *J. Climate*, **26**, 1268–1285, doi:10.1175/JCLI-D-12-00057.1.

Lau, N.-C., and M. J. Nath, 1996: The role of the "atmospheric bridge" in linking tropical Pacific ENSO events to extratropical SST anomalies. *J. Climate*, **9**, 2036–2057, doi:10.1175/1520-0442(1996)009<2036:TROTBI>2.0.CO;2.

Lee, M.-Y., C.-C. Hong, and H.-H. Hsu, 2015: Compounding effects of warm SST and reduced sea ice on the extreme

circulation over the extratropical North Pacific and North America during the 2013–2014 boreal winter. *Geophys. Res. Lett.*, **42**, 1612–1618, doi:10.1002/2014GL062956.

Namias, J., and R. M. Born, 1970: Temporal coherence in North Pacific sea-surface temperature patterns. *J. Geophys. Res.*, **75**, 5952–5955, doi:10.1029/JC075i030p05952.

Newman, M., and Coauthors, 2016: The Pacific decadal oscillation, revisited. *J. Climate*, **29**, 4399–4427, doi:10.1175/JCLI-D-15-0508.1.

Peng, P., A. Kumar, and W. Wang, 2011: An analysis of seasonal predictability in coupled model forecasts. *Climate Dyn.*, **36**, 637–648, doi:10.1007/s00382-009-0711-8.

Saha, S., and Coauthors, 2010: The NCEP Climate Forecast System Reanalysis. *Bull. Amer. Meteor. Soc.*, **91**, 1015–1057, doi:10.1175/2010BAMS3001.1.

——, and Coauthors, 2014: The NCEP Climate Forecast System version 2. *J. Climate*, **27**, 2185–2208, doi:10.1175/JCLI-D-12-00823.1.

Schneider, E. K., L. Bengtsson, and Z.-Z. Hu, 2003: Forcing of Northern Hemisphere climate trends. *J. Atmos. Sci.*, **60**, 1504–1521, doi:10.1175/1520-0469(2003)060<1504:FONHCT>2.0.CO;2.

Seager, R., M. Hoerling, S. Schubert, H. Wang, B. Lyon, A. Kumar, J. Nakamura, and N. Henderson, 2015: Causes of the 2011–14 California drought. *J. Climate*, **28**, 6997–7024, doi:10.1175/JCLI-D-14-00860.1.

Watson, P. A. G., A. Weisheimer, J. R. Knight, and T. N. Palmer, 2016: The role of the tropical West Pacific in the extreme Northern Hemisphere winter of 2013/2014. *J. Geophys. Res. Atmos.*, **121**, 1698–1714, doi:10.1002/2015JD024048.

Wen, C., Y. Xue, and A. Kumar, 2012: Seasonal prediction of North Pacific SSTs and PDO in the NCEP CFS hindcasts. *J. Climate*, **25**, 5689–5710, doi:10.1175/JCLI-D-11-00556.1.

Xue, Y., M. Chen, A. Kumar, Z.-Z. Hu, and W. Wang, 2013: Prediction skill and bias of tropical Pacific sea surface temperatures in the NCEP Climate Forecast System version 2. *J. Climate*, **26**, 5358–5378, doi:10.1175/JCLI-D-12-00600.1.

——, Z.-Z. Hu, A. Kumar, V. Banzon, T. M. Smith, and N. A. Rayner, 2015: Sea surface temperatures [in "State of the Climate in 2014"]. *Bull. Amer. Meteor. Soc.*, **96** (7), S59–S64.

——, ——, ——, ——, B. Huang, and J. Kennedy, 2016: Sea surface temperatures [in "State of the Climate in 2015"]. *Bull. Amer. Meteor. Soc.*, **97** (8), S63–S66.

Zhu, J., B. Huang, L. Marx, J. L. Kinter III, M. A. Balmaseda, R.-H. Zhang, and Z.-Z. Hu, 2012: Ensemble ENSO hindcasts initialized from multiple ocean analyses. *Geophys. Res. Lett.*, **39**, L09602, doi:10.1029/2012GL051503.